Structural and Multidisciplinary Optimization (2018) 58:475–487
https://doi.org/10.1007/s00158-018-1898-2

RESEARCH PAPER

A method for topology optimization of structures under harmonic excitations

Xuqi Zhao[1] · Baisheng Wu[2] · Zhengguang Li[1] · Huixiang Zhong[3]

Received: 17 May 2017 / Revised: 8 November 2017 / Accepted: 2 January 2018 / Published online: 16 January 2018

Abstract
This paper deals with topology optimization of large-scale structures with proportional damping subjected to harmonic excitations. A combined method (CM) of modal superposition with model order reduction (MOR) for harmonic response analysis is introduced. In the method, only the modes corresponding to a frequency range which is a little bigger than that of interest are used for modal superposition, the contribution of unknown higher modes is complemented by a MOR technique. Objective functions are the integral of dynamic compliance of a structure, and that of displacement amplitude of a certain user-defined degree of freedom in the structure, over a range of interested frequencies. The adjoint variable method is applied to analyze sensitivities of objective functions and the accuracy of the sensitivity analyses can also be ensured by CM. Topology optimization procedure is illustrated by three examples. It is shown that the topology optimization based on CM not only remarkably reduce CPU time, but also ensure accuracy of results.

Keywords Topology optimization · Harmonic response · Modal superposition · Model order reduction

1 Introduction

Structural topology optimization is a method to find the optimal distribution of material within an admissible design domain (Bendsøe and Kikuchi 1988). It is applied to a wide range of structural design problems (Bendsøe and Sigmund 2004; Deaton and Grandhi 2014). For dynamic problems, researches mainly focus on three aspects such as topology optimization of natural frequency (Díaz and Kikuchi 1992; Pedersen 2000; Du and Olhoff 2007), topology optimization of dynamic response in the time domain (Zhao and Wang 2016) and frequency domain (Ma et al. 1995; Jog 2002; Shu et al. 2011).

This paper is mainly concerned with the third case, i.e. structural topology optimization under harmonic excitations. Recently, many researchers study this kind of problems. Ma et al. (1995) used homogenization method to investigate topology optimization of harmonic response problems. Jog (2002) firstly introduced "dynamic compliance" as an objective function of topology optimization based on density method. Tcherniak (2002) formulated an optimization problem of maximization of the magnitude of steady-state vibrations for a given frequency. Olhoff and Du (2005) focused on minimizing dynamic compliance of undamped systems at a given frequency. Jensen (2007) employed the Padé approximation method to solve harmonic response in structural topology optimization. Yoon (2010) studied structural topology optimization related to dynamic responses by using model reduction schemes such as mode superposition, Ritz vector, and quasi-static Ritz vector methods. Some works (Kang et al. 2012; Yu et al. 2013; Zhu et al. 2017) focused on practical applications

✉ Baisheng Wu
wubs@gdut.edu.cn

Xuqi Zhao
kevin-sh2010@hotmail.com

Zhengguang Li
lizg@jlu.edu.cn

Huixiang Zhong
zhonghx@jlu.edu.cn

[1] School of Mathematics, Jilin University, Changchun 130012, People's Republic of China

[2] School of Electro-Mechanical Engineering, Guangdong University of Technology, Guangzhou 510006, People's Republic of China

[3] College of Computer Science and Technology, Jilin University, Changchun 130012, People's Republic of China

of structural topology optimization under harmonic excitations. For large-scale problems, Liu et al. (2015) made a comparative study among mode displacement method (MDM), mode acceleration method (MAM) and full method (FM) for structural topology optimization under harmonic excitations. It concludes that MAM is a preferable method, compared with MDM, due to its balance between efficiency and accuracy.

However, MAM lacks a straightforward procedure to control the accuracy of structural harmonic response analysis, it cannot also determine the number of lower eigenfrequencies and eigenvectors required for modal superposition. Generally, optimization process involves repeated analysis of harmonic response. Hence, an efficient method is required to deal with large-scale harmonic response problems for structural topology optimization. On the other hand, in the adjoint variable method (AVM) (Haftka and Gürdal 1992; Yoon 2010) for computing the sensitivities of objective functions related to harmonic response, the corresponding analysis method is again used to obtain the adjoint variable vector. The accuracy of harmonic response analysis is thus another critical aspect. Therefore, a more accurate, controllable and efficient method for harmonic response analysis is needed. In this paper, a combined method (CM) (Wu et al. 2015b) of modal superposition with model order reduction (MOR) is introduced to compute harmonic response for a range of interested frequencies. By using the Sturm sequence, the method can self-adaptively determine the number of lower modes for modal superposition instead of fixing the number in the MAM, as modes re-distribute due to updating of design variables. The MOR method is used to ensure the accuracy owing to lacking of unknown higher modes.

The paper is organized as follow. Section 2 introduces two methods for computing harmonic response of structures under harmonic excitations, including CM (Wu et al. 2015b) and MAM. In section 3, we review formulations of topology optimization and sensitivity analysis based on AVM. In section 4, three examples are given and comparison of topology optimization results based on CM and MAM is performed to demonstrate accuracy and efficiency of the proposed method. Conclusions are presented in Section 5.

2 Methods of harmonic response analysis

The governing equation of a discretized structure with n DOFs under harmonic loading can be written as

$$\mathbf{M}\ddot{\mathbf{X}}(t)+\mathbf{C}\dot{\mathbf{X}}(t)+\mathbf{K}\mathbf{X}(t)=\mathbf{F}(t)=\mathbf{F}e^{i\omega t},\omega\in[0,\omega_f] \quad (1)$$

where $\mathbf{M}$, $\mathbf{C}$, $\mathbf{K}$ represent the mass matrix, damping matrix and stiffness matrix, respectively, and $\mathbf{M}$, $\mathbf{K}$ are symmetric positive definite; $\mathbf{X}(t)$ represents the displacement vector; $\mathbf{F}=\mathbf{F}_1+i\mathbf{F}_2$ represents vector of amplitudes and phases of the harmonic external force, $\mathbf{F}_1$ and $\mathbf{F}_2$ are real vectors; ω is the excitation frequency. In this paper, proportional damping $\mathbf{C}=\alpha\mathbf{M}+\beta\mathbf{K}$ is considered where α, β are damping coefficients of the structure. Assume that $\mathbf{X}(t)=\mathbf{x}e^{i\omega t}$ is the solution of (1), its substitution into (1) yields

$$\left(\mathbf{K}+i\omega\mathbf{C}-\omega^2\mathbf{M}\right)\mathbf{x}=\mathbf{F},\quad \omega\in[0,\omega_f] \quad (2)$$

Note that, every evaluation of $\mathbf{x}(\omega)$ requires solving (2), and for a large-scale system, the FM for every frequency of interest within $[0,\omega_f]$ is usually unaffordable. For this reason, the FM is unsuitable as a method of harmonic response analysis with multiple excitation frequencies for structural topology optimization.

2.1 A combined method of modal superposition with model order reduction

Wu et al. (2015b) presented a combined method of modal superposition with MOR for harmonic response analysis of structures. This method allows very fast development of approximate solutions of high quality and low computational cost. It is applicable for topology optimization of structures under harmonic excitations which involves many times of harmonic response computation. The method is briefly described as follows.

Let $\mathbf{x}_1$ and $\mathbf{x}_2$ be solutions to the following two systems, respectively

$$\begin{cases}\left(\mathbf{K}+i\omega\mathbf{C}-\omega^2\mathbf{M}\right)\mathbf{x}_1=\mathbf{F}_1\\ \left(\mathbf{K}+i\omega\mathbf{C}-\omega^2\mathbf{M}\right)\mathbf{x}_2=\mathbf{F}_2\end{cases} \quad (3)$$

for $\omega\in[0,\omega_f]$ where $\mathbf{x}_1$ and $\mathbf{x}_2$ are complex vectors. Hence, the solution of (2) $\mathbf{x}$ can be written as

$$\mathbf{x}=\mathbf{x}_1+i\mathbf{x}_2 \quad (4)$$

Based on the modal superposition method, $\mathbf{x}_1$ in (3) can be expressed as

$$\mathbf{x}_1=\mathbf{\Phi}\mathbf{y}_1 \quad (5)$$

where $\mathbf{y}_1=(y_1^1,\ldots,y_n^1)^{\mathrm{T}}$, $y_j^1=\frac{\boldsymbol{\varphi}_j^{\mathrm{T}}\mathbf{F}_1}{\omega_j^2-\omega^2+i\alpha\omega+i\beta\omega_j^2\omega}(j=1,\ldots,n)$, $\mathbf{\Phi}=[\boldsymbol{\varphi}_1,\ldots,\boldsymbol{\varphi}_n]$, $\boldsymbol{\varphi}_j$ and ω_j $(j=1,\ldots,n)$ are eigenvectors and eigenfrequencies of the undamped system which satisfy

$$\begin{cases}\mathbf{K}\boldsymbol{\varphi}_i=\omega_i^2\mathbf{M}\boldsymbol{\varphi}_i\\ \boldsymbol{\varphi}_j^{\mathrm{T}}\mathbf{M}\boldsymbol{\varphi}_i=\delta_{ij}\end{cases},\quad i,j=1,\ldots,n \quad (6)$$

where δ_{ij} is Kronecker delta, ω_i is in rad/s. Taking the computational efficiency into account, only lower l eigenfrequencies and eigenvectors are computed (l is far less than n and $\omega_l>\omega_f$). The Sturm sequence (Bathe 2014) can be used to determine l before the computation of eigenproblem, i.e. $\mathbf{K}-\omega_f^2\mathbf{M}=\mathbf{L}\mathbf{D}_f\mathbf{L}^{\mathrm{T}}$, $l=n_f+1$, where n_f is the number of negative elements in $\mathbf{D}_f$.

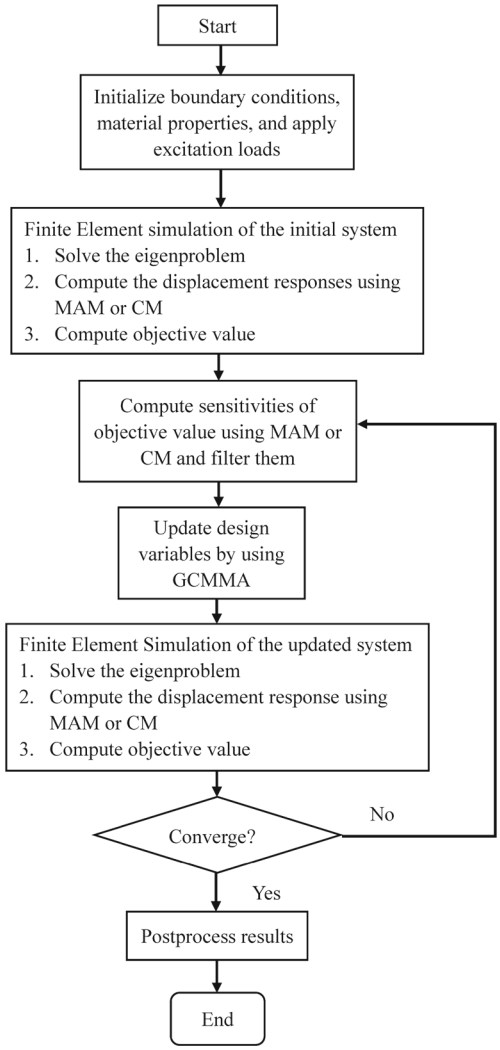

Fig. 1 The flow chart of the optimization procedure

Eq. (5) can be written as follow

$$\mathbf{x}_1 = \mathbf{\Phi}_{\mathrm{L}}\tilde{\mathbf{y}}_1 + \mathbf{\Phi}_{\mathrm{H}}\mathbf{c}_1 \tag{7}$$

where $\tilde{\mathbf{y}}_1 = \left(\tilde{y}_1^1, \tilde{y}_2^1, \ldots, \tilde{y}_l^1\right)^{\mathrm{T}}, \tilde{y}_j^1 = \frac{\boldsymbol{\varphi}_j^{\mathrm{T}}\mathbf{F}_1}{\omega_j^2 - \omega^2 + i\alpha\omega + i\beta\omega_j^2\omega}\ (j = 1, \ldots, l)$, $\mathbf{\Phi}_{\mathrm{L}} = [\boldsymbol{\varphi}_1, \ldots, \boldsymbol{\varphi}_l]$ and $\mathbf{\Phi}_{\mathrm{H}}$ are the unknown higher eigenvectors.

Fig. 2 2D cantilever beam

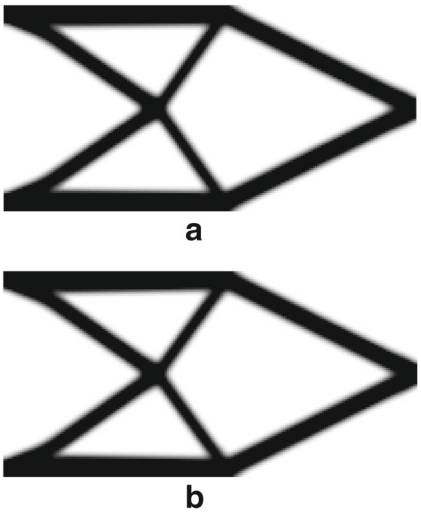

Fig. 3 **a** The converged result of Example 1 using CM for [0,50]Hz. **b** The converged result of Example 1 using MAM for [0,50]Hz

The unknown part of $\mathbf{x}_1$ can be written as $\mathbf{w}_1 = \mathbf{\Phi}_{\mathrm{H}}\mathbf{c}_1$ and it satisfies the following equation

$$\begin{aligned}
&(\mathbf{K} + i\omega\mathbf{C} - \omega^2\mathbf{M})\mathbf{w}_1 = \mathbf{F}_1 - (\mathbf{K} + i\omega\mathbf{C} - \omega^2\mathbf{M})\mathbf{\Phi}_{\mathrm{L}}\tilde{\mathbf{y}}_1 \\
&= \mathbf{F}_1 - \left(\sum_{j=1}^{l}\tilde{y}_j^1\mathbf{K}\boldsymbol{\varphi}_j + i\alpha\omega\sum_{j=1}^{l}\tilde{y}_j^1\mathbf{M}\boldsymbol{\varphi}_j + i\beta\omega\sum_{j=1}^{l}\tilde{y}_j^1\mathbf{K}\boldsymbol{\varphi}_j - \omega^2\sum_{j=1}^{l}\tilde{y}_j^1\mathbf{M}\boldsymbol{\varphi}_j\right) \\
&= \mathbf{F}_1 - \left(\sum_{j=1}^{l}\omega_j^2\tilde{y}_j^1\mathbf{M}\boldsymbol{\varphi}_j + i\alpha\omega\sum_{j=1}^{l}\tilde{y}_j^1\mathbf{M}\boldsymbol{\varphi}_j + i\beta\omega\sum_{j=1}^{l}\omega_j^2\tilde{y}_j^1\mathbf{M}\boldsymbol{\varphi}_j - \omega^2\sum_{j=1}^{l}\tilde{y}_j^1\mathbf{M}\boldsymbol{\varphi}_j\right), \omega\in[0,\omega_f] \\
&= \mathbf{F}_1 - \left\{\sum_{j=1}^{l}\tilde{y}_j^1\left(\omega_j^2 - \omega^2 + i\omega\alpha + i\omega\omega_j^2\beta\right)\mathbf{M}\boldsymbol{\varphi}_j\right\} \\
&= \mathbf{F}_1 - \sum_{j=1}^{l}\boldsymbol{\varphi}_j^{\mathrm{T}}\mathbf{F}_1\mathbf{M}\boldsymbol{\varphi}_j = \mathbf{F}_1 - \mathbf{M}\mathbf{\Phi}_{\mathrm{L}}\mathbf{\Phi}_{\mathrm{L}}^{\mathrm{T}}\mathbf{F}_1, \omega\in[0,\omega_f]
\end{aligned} \tag{8}$$

It is impossible to compute all the unknown higher eigenvectors for large-scale structures. A feasible scheme is to construct an approximate solution of (8) by projecting it onto a subspace spanned by the columns of $\mathbf{V}_1 \in \mathbf{R}^{n\times m}$ with dimension m far less than $n - l$, i.e.

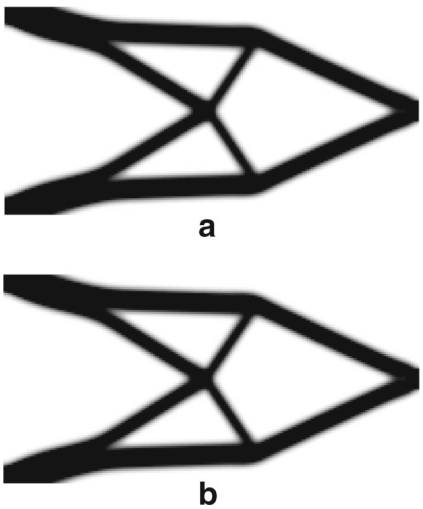

Fig. 4 **a** The converged result of Example 1 using CM for [0,100]Hz. **b** The converged result of Example 1 using MAM for [0,100]Hz

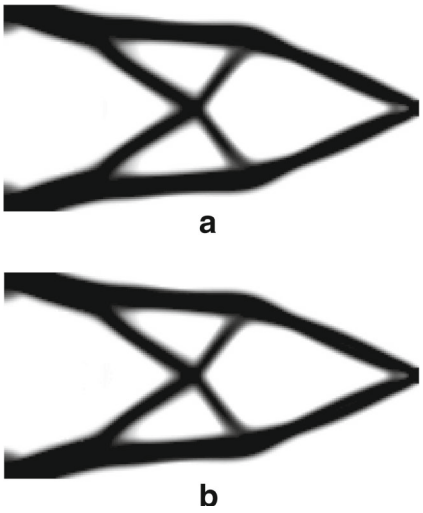

Fig. 5 **a** The converged result of Example 1 using CM for [0,500]Hz. **b** The converged result of Example 1 using MAM for [0,500]Hz

$$\mathbf{w}_1 = \mathbf{V}_1\mathbf{z}_1 \tag{9}$$

where $\mathbf{z}_1 \in \mathbf{C}^m$ is the complex vector of generalized coordinates.

Due to the feature of proportional damping, the first equation of (3) can be decoupled by the eigenvectors of (6). Hence, it is natural to construct the subspace $\mathbf{V}_1$ from the undamped system ($\alpha = 0, \beta = 0$) resulted from (8), i.e.

$$\left(\mathbf{K}-\omega^2\mathbf{M}\right)\tilde{\mathbf{w}}_1 = \mathbf{F}_1-\mathbf{M}\boldsymbol{\Phi}_\mathrm{L}\boldsymbol{\Phi}_\mathrm{L}^\mathrm{T}\mathbf{F}_1, \quad \omega\in\left[0,\omega_f\right] \tag{10}$$

Preconditioned Conjugate Gradients (PCG) method is an efficient algorithm to solve large sparse linear positive definite systems. Note that the coefficient matrix $\mathbf{K}-\omega^2\mathbf{M}$ is symmetric, but not positive definite. In order to apply PCG algorithm, the coefficient matrix should be equivalently transformed to a symmetric positive definite matrix. The solution of (10) can be written as follow

$$\tilde{\mathbf{w}}_1 = \boldsymbol{\Phi}_\mathrm{H}\tilde{\mathbf{c}}_1 \tag{11}$$

where $\tilde{\mathbf{c}}_1 = [\tilde{c}_{l+1}, \ldots, \tilde{c}_n]^\mathrm{T}$, $\tilde{c}_j = \frac{\boldsymbol{\varphi}_j^\mathrm{T}\mathbf{F}_1}{\omega_j^2-\omega^2}$ $(j = l+1, \ldots, n)$. Due to the orthogonality of eigenvectors, one has $\boldsymbol{\Phi}_\mathrm{L}^\mathrm{T}\mathbf{M}\boldsymbol{\Phi}_\mathrm{H} = \mathbf{0}$. Hence, $\tilde{\mathbf{w}}_1$ is $\mathbf{M}$ orthogonal with respect to $\boldsymbol{\Phi}_\mathrm{L}$. As a result, $\tilde{\mathbf{w}}_1$ satisfies the following equation

Table 1 Performance results of topology optimization based on MAM and CM for Example 1: [0,50]Hz

Method	Initial objective value	Converged objective value	CPU time(s)	Iteration number
MAM	10.1609	0.1820	8240.33	187
CM	10.1614	0.1813	2456.13	205

Table 2 Performance results of topology optimization based on MAM and CM for Example 1: [0,100]Hz

Method	Initial objective value	Converged objective value	CPU time(s)	Iteration number
MAM	12.6037	0.4155	8998.47	208
CM	12.6052	0.4162	3103.84	203

$$\left[\mathbf{K}-\omega^2\mathbf{M}+\omega^2\mathbf{M}\boldsymbol{\Phi}_\mathrm{L}(\mathbf{M}\boldsymbol{\Phi}_\mathrm{L})^\mathrm{T}\right]\tilde{\mathbf{w}}_1 = \left[\mathbf{K}-\omega^2\mathbf{M}\right]\tilde{\mathbf{w}}_1 = \mathbf{F}_1-\mathbf{M}\boldsymbol{\Phi}_\mathrm{L}\boldsymbol{\Phi}_\mathrm{L}^\mathrm{T}\mathbf{F}_1, \omega\in\left[0,\omega_f\right] \tag{12}$$

The coefficient matrix $\mathbf{K}-\omega^2\mathbf{M}+\omega^2\mathbf{M}\boldsymbol{\Phi}_\mathrm{L}(\mathbf{M}\boldsymbol{\Phi}_\mathrm{L})^\mathrm{T}$ is symmetric and positive definite (Wu et al. 2015b). Hence, PCG (Golub and Van Loan 2013) method may be applied to solve (12).

Because the computation of eigenfrequencies and eigenvectors is generally performed by using iterative methods such as Lanczos (Grimes et al. 1994) or subspace method (Bathe 2013), the factorized stiffness matrix $\mathbf{K} = \mathbf{U}^\mathrm{T}\mathbf{U}$ is available and is chosen as the preconditioner. Now, the PCG method is applied to solve (12) with $\omega = \omega_f$, i.e.

$$\left[\mathbf{K}-\omega_f^2\mathbf{M}+\omega_f^2\mathbf{M}\boldsymbol{\Phi}_\mathrm{L}(\mathbf{M}\boldsymbol{\Phi}_\mathrm{L})^\mathrm{T}\right]\tilde{\mathbf{w}}_1 = \mathbf{F}_1-\mathbf{M}\boldsymbol{\Phi}_\mathrm{L}\boldsymbol{\Phi}_\mathrm{L}^\mathrm{T}\mathbf{F}_1 \tag{13}$$

to yield the search directions $\mathbf{v}_j (j = 1, 2, \cdots, m)$ and form the subspace $\mathbf{V}_1 = [\mathbf{v}_1, \ldots, \mathbf{v}_m]$. Here, $\mathbf{v}_j$ is normalized by $\|\mathbf{v}_j\|_2 = 1$ $(j = 1, 2, \cdots, m)$. The PCG algorithm will terminate if the 2-norm of relative residual vector $\mathbf{r}_m$ of mth step reaches the error tolerance, i.e. $\|\mathbf{r}_m\|_2/\|\mathbf{F}\|_2 < \varepsilon$, where $\|\mathbf{F}\|_2 = \sqrt{\|\mathbf{F}_1\|_2^{\,2} + \|\mathbf{F}_2\|_2^{\,2}}$, ε is the error tolerance.

Note that, for a proportional damping system, the harmonic response can be represented by the eigenvectors of the corresponding undamped system, for example, see (2). Since $\mathbf{V}_1$ is the Krylov subspace constructed by solving (13) and it is an approximation to the unknown higher eigenvectors $\boldsymbol{\Phi}_\mathrm{H}$. Such a $\mathbf{V}_1$ can be used to implement Galerkin projection for the complementary part of contribution of computed eigenvectors. Setting $\omega = \omega_f$ in (12) is equivalent to using a best shift for constructing an fast approximation to $\boldsymbol{\Phi}_\mathrm{H}$. If a small or larger value of ω is selected for obtaining the subspace $\mathbf{V}_1$, the convergence speed of CM method will be affected.

Table 3 Performance results of topology optimization based on MAM and CM for Example 1: [0,500]Hz

Method	Initial objective value	Converged objective value	CPU time(s)	Iteration number
MAM	14.1862	1.9396	15053.16	176
CM	14.2892	1.9806	11757.25	171

Table 4 Details of time distribution for computing harmonic response by CM at the initial step for the three frequency intervals in Example 1

Frequency interval	Sturm sequence(s)	Number of lower modes	Solution of the eigenproblem(s)	PCG method(s)	Calculation of (14) and (16)(s)	Total(s)
[0,50]Hz	0.869	2	1.764	0.090	0.258	2.981
[0,100]Hz	0.842	2	1.593	0.115	0.378	2.928
[0,500]Hz	0.836	7	3.618	0.167	1.785	6.406

Next, perform Galerkin projection of (8) by using subspace $\mathbf{V}_1$ and solve reduced order system to obtain the vector $\mathbf{z}_1$ at each frequency of interest

$$\left(\mathbf{K}_r + i\omega\mathbf{C}_r - \omega^2\mathbf{M}_r\right)\mathbf{z}_1 = \mathbf{F}_r, \quad \omega \in [0, \omega_f] \tag{14}$$

where the subscript r denotes reduced system:

$$\mathbf{K}_r = \mathbf{V}_1^{\mathrm{T}}\mathbf{K}\mathbf{V}_1, \mathbf{M}_r = \mathbf{V}_1^{\mathrm{T}}\mathbf{M}\mathbf{V}_1, \mathbf{C}_r = \alpha\mathbf{M}_r + \beta\mathbf{K}_r, \mathbf{F}_r = \mathbf{V}_1^{\mathrm{T}}\left(\mathbf{F}_1 - \mathbf{M}\boldsymbol{\Phi}_{\mathrm{L}}\boldsymbol{\Phi}_{\mathrm{L}}^{\mathrm{T}}\mathbf{F}_1\right) \tag{15}$$

Finally, the approximate solution to the first equation of (3) can be written as

$$\mathbf{x}_{1a} = \boldsymbol{\Phi}_{\mathrm{L}}\mathbf{c}_1 + \mathbf{V}_1\mathbf{z}_1, \omega \in [0, \omega_f] \tag{16}$$

For a system with large damping effect, the subspace $\mathbf{V}_1$ can be constructed in a similar way by simply changing convergence criteria (Wu et al. 2016) to $\|(\mathbf{K} + i\omega_f\mathbf{C} - \omega_f^2\mathbf{M})\mathbf{x}_{1a} - \mathbf{F}_1\| \le \varepsilon\|\mathbf{F}_1\|$ where $\mathbf{x}_{1a}$ is given in (16).

Summarily, the harmonic response vector $\mathbf{x}(\omega)$ can be obtained by the following computation procedure

1. Use the Sturm sequence to determine the number l ($\omega_l > \omega_f$).
2. Solve the eigenproblem to obtain the lower l eigenfrequencies and eigenvectors, and store the upper triangular part $\mathbf{U}$of the factorized stiffness matrix $\mathbf{K} = \mathbf{U}^{\mathrm{T}}\mathbf{U}$.
3. Apply PCG algorithm and use the factorized stiffness matrix as the preconditioner to solve (13), and obtain reduction bases $\mathbf{V}_1 = [\mathbf{v}_1, \mathbf{v}_2, \ldots, \mathbf{v}_m]$.
4. Compute reduced system matrices $\mathbf{K}_r$, $\mathbf{M}_r$, and vector $\mathbf{F}_r$in (15).
5. Compute $\mathbf{z}_1$ for each frequency of interest ω in $[0, \omega_f]$ by solving (14) and get $\mathbf{x}_{1a}$ by (16).
6. Compute $\mathbf{x}_{2a}$ by the same method, and finally obtain $\mathbf{x}_a = \mathbf{x}_{1a} + i\mathbf{x}_{2a}$.
7. The relative residual errors (RRE) is used to measure the accuracy of proposed method.

$$\mathrm{RRE} = \frac{\left\|(\mathbf{K} + i\omega\mathbf{C} - \omega^2\mathbf{M})\mathbf{x}_a(\omega) - \mathbf{F}\right\|_2}{\|\mathbf{F}\|_2} \tag{17}$$

Table 5 Details of time distribution for computing harmonic response by MAM at the initial step for the three frequency intervals in Example 1

Frequency interval	Number of lower modes	Solution of the eigenproblem(s)	Solution of (22)(s)	Total(s)
[0,50]Hz	20	11.356	0.210	11.566
[0,100]Hz	20	11.568	0.262	11.830
[0,500]Hz	20	11.103	0.720	11.823

2.2 Mode acceleration method

Usually, modal acceleration method (Dickens et al. 1997) is applied to compute harmonic response for structural topology optimization. This part gives an outline of MAM. Based on the modal superposition method, the solution of (2) can be written as

$$\mathbf{x} = \sum_{j=1}^{n} \boldsymbol{\varphi}_j y_j = \boldsymbol{\Phi}\mathbf{y} \tag{18}$$

where.

$$\boldsymbol{\Phi} = [\boldsymbol{\varphi}_1, \ldots, \boldsymbol{\varphi}_n], \ \mathbf{y} = [y_1, \ldots, y_n]^{\mathrm{T}}, \ y_j = \frac{\boldsymbol{\varphi}_j^{\mathrm{T}}\mathbf{F}}{\omega_j^2 - \omega^2 + i\omega\alpha + i\omega\omega_j^2\beta}$$

($j = 1, \ldots, n$).

The solution in (18) can be written as follow

$$\mathbf{x} = \mathbf{K}^{-1}\mathbf{F} + \boldsymbol{\Phi}\mathbf{y} - \mathbf{K}^{-1}\mathbf{F} \tag{19}$$

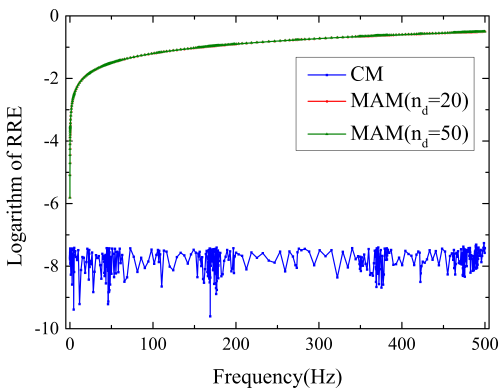

Fig. 6 The comparison of RREs of harmonic responses by MAM and CM at the initial step for Example 1: [0,500]Hz

Table 6 The relative errors of the sensitivity analysis by CM and MAM at the initial step for Example 1

Method	[0,50]Hz	[0,100]Hz	[0,500]Hz
CM	2.939e-09	1.861e-08	5.498e-09
MAM	1.217e-04	2.287e-03	0.3671

Note that the inverse of the stiffness matrix $\mathbf{K}$ can be represented as

$$\mathbf{K}^{-1} = \mathbf{\Phi}\mathbf{\Lambda}^{-1}\mathbf{\Phi}^{\mathrm{T}} \tag{20}$$

where $\mathbf{\Lambda} = diag\left(\omega_1^2, \ldots, \omega_n^2\right)$. The substitution of (20) in the third part of (19) yields

$$\mathbf{x} = \mathbf{K}^{-1}\mathbf{F} + \mathbf{\Phi}\mathbf{y} - \mathbf{\Phi}\mathbf{\Lambda}^{-1}\mathbf{\Phi}^{\mathrm{T}}\mathbf{F} \tag{21}$$

However, taking the computational efficiency into account, only lower n_d eigenfrequencies and eigenvectors are computed for large-scale problems. Hence, an approximate solution to (2) may be written as follows

$$\tilde{\mathbf{x}}_a = \mathbf{K}^{-1}\mathbf{F} + \mathbf{\Phi}_{n_d}\mathbf{y}_{n_d} - \mathbf{\Phi}_{n_d}\mathbf{\Lambda}_{n_d}^{-1}\mathbf{\Phi}_{n_d}^{\mathrm{T}}\mathbf{F} \tag{22}$$

It can be derived that

$$\begin{aligned}\tilde{\mathbf{x}}_a &= \mathbf{\Phi}_{n_d}\mathbf{y}_{n_d} + \sum_{k=n_d+1}^{n}\frac{\boldsymbol{\varphi}_k\boldsymbol{\varphi}_k^{\mathrm{T}}\mathbf{F}}{\omega_k^2} \\ &= \mathbf{\Phi}\mathbf{y} + \sum_{k=n_d+1}^{n}\left(\frac{\boldsymbol{\varphi}_k\boldsymbol{\varphi}_k^{\mathrm{T}}\mathbf{F}}{\omega_k^2} - \frac{\boldsymbol{\varphi}_k\boldsymbol{\varphi}_k^{\mathrm{T}}\mathbf{F}}{\omega_k^2 - \omega^2 + i\omega\alpha + i\omega\omega_k^2\beta}\right)\end{aligned} \tag{23}$$

where $\mathbf{\Lambda}_{n_d} = diag\left(\omega_1^2, \ldots, \omega_{n_d}^2\right)$, $\mathbf{\Phi}_{n_d} = \left[\boldsymbol{\varphi}_1, \ldots, \boldsymbol{\varphi}_{n_d}\right]$ are lower n_d computed eigenfrequencies and eigenvectors for MAM and $\mathbf{y}_{n_d} = \left(y_1, \ldots, y_{n_d}\right)^{\mathrm{T}}$. The first part of (23) is the exact solution of (2), and its second part is the error vector of MAM, ω_k and $\boldsymbol{\varphi}_k (k = n_d + 1, \ldots, n)$ are the unknown part of eigenfrequencies and eigenvectors of (6). Generally, n_d is far less than n and can be chosen by experience in the application. When the excitation frequency $\omega = 0$, the term $\frac{\boldsymbol{\varphi}_k\boldsymbol{\varphi}_k^{\mathrm{T}}\mathbf{F}}{\omega_k^2} - \frac{\boldsymbol{\varphi}_k\boldsymbol{\varphi}_k^{\mathrm{T}}\mathbf{F}}{\omega_k^2 - \omega^2 + i\omega\alpha + i\omega\omega_k^2\beta}$ is equal to 0. As the excitation frequency ω increases, the level of $\frac{\boldsymbol{\varphi}_k\boldsymbol{\varphi}_k^{\mathrm{T}}\mathbf{F}}{\omega_k^2 - \omega^2 + i\omega\alpha + i\omega\omega_k^2\beta}$ deviating from $\frac{\boldsymbol{\varphi}_k\boldsymbol{\varphi}_k^{\mathrm{T}}\mathbf{F}}{\omega_k^2}$ increases. As a result, when n_d is determined, the error will increase as ω increases. It means that MAM may not ensure the accuracy at a higher excitation frequency ω. Furthermore, Example 1 in Section 4 will demonstrate that attempts to increase n_d may not cause a remarkable improvement of accuracy. RRE is also used to measure the accuracy of MAM.

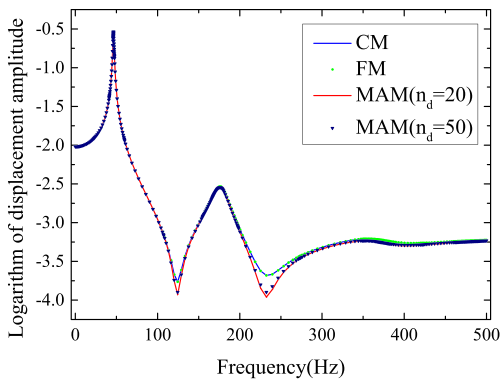

Fig. 7 The comparison of displacement amplitudes of the user-defined DOF at the initial step for Example 1: [0,500]Hz

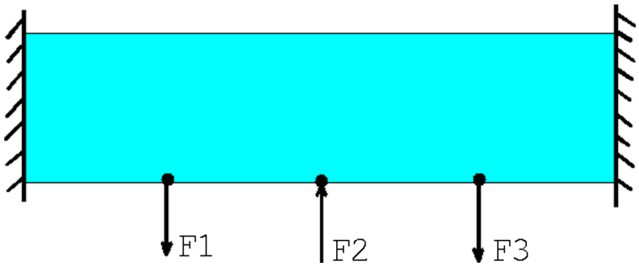

Fig. 8 2D double clamped structure

3 Topology optimization formulation

For the dynamic response under harmonic excitations, the formulation of topology optimization can be stated as

$$\begin{aligned} &find\ 0 < \underline{\rho} \le \rho_e \le 1, \quad e = 1, \ldots, n_e \\ &\min \int_0^{\omega_f} \|J(\omega)\| d\omega \\ &\text{s.t.} \sum_{e=1}^{n_e} \rho_e v_e \le V \end{aligned} \tag{24}$$

where ρ_e is the pseudo-density of element e and it is the design variable in the problem, $\underline{\rho} = 0.001$ is the lower bound of design variable, V is the prescribed total volume of available material, and n_e presents the total number of finite elements. The function $\|J(\omega)\|$ is as follow

$$\|J(\omega)\| = \sqrt{J(\omega)\overline{J}(\omega)} = \left\|\mathbf{L}^{\mathrm{T}}\mathbf{x}(\omega)\right\|_2 \tag{25}$$

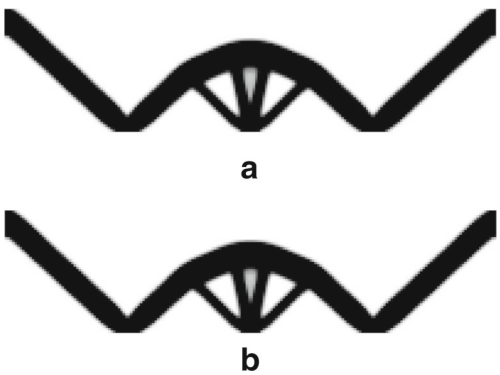

Fig. 9 **a** The converged result of topology optimization based on CM for Example 2: [0,50]Hz. **b** The converged result of topology optimization based on MAM for Example 2: [0,50]Hz

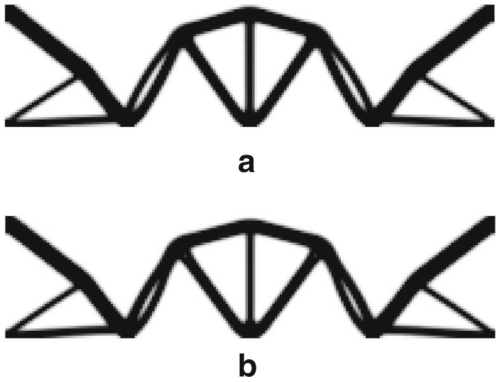

Fig. 10 **a** The converged result of topology optimization based on CM for Example 2: [0,500]Hz**. b** The converged result of topology optimization based on MAM for Example 2: [0,500]Hz

where $\overline{J}(\omega)$ is complex conjugate of $J(\omega)$. For the problem of dynamic compliance suggested by Ma et al. (1995), Jensen (2007) and Yoon (2010), the vector **L** in (25) is equal to **F** in (2). On the other hand, for the problem of amplitude minimization of a certain user-defined DOF in the structure (Yoon 2010; Liu et al. 2015), the vector **L** is a column vector with the value of 1 at term s and zeros otherwise which s means the user-defined DOF in the structure.

In order to ensure the accuracy, the integral of (24) in a frequency interval is divided into some subdivisions to implement. The determination of subdivisions (Liu et al. 2015) depends on eigenfrequencies of (6), because the harmonic response sharply jumps around them. Hence, the interval between adjacent eigenfrequencies (ω_{i-1} and ω_i) are divided into 6 subdivisions as follows

$$\begin{aligned}
&[\omega_{i-1}, \omega_{i-1} + 0.01(\omega_i - \omega_{i-1})]\\
&[\omega_{i-1} + 0.01(\omega_i - \omega_{i-1}), \omega_{i-1} + 0.11(\omega_i - \omega_{i-1})]\\
&[\omega_{i-1} + 0.11(\omega_i - \omega_{i-1}), \omega_{i-1} + 0.50(\omega_i - \omega_{i-1})]\\
&[\omega_{i-1} + 0.50(\omega_i - \omega_{i-1}), \omega_{i-1} + 0.89(\omega_i - \omega_{i-1})]\\
&[\omega_{i-1} + 0.89(\omega_i - \omega_{i-1}), \omega_{i-1} + 0.99(\omega_i - \omega_{i-1})]\\
&[\omega_{i-1} + 0.99(\omega_i - \omega_{i-1}), \omega_i]
\end{aligned} \tag{26}$$

Gauss-Legendre integration is used to calculate the integral in a subdivision.

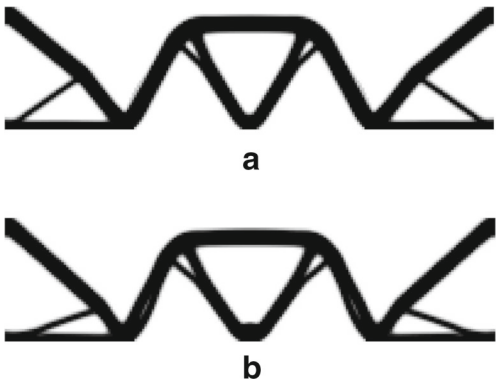

Fig. 11 **a** The converged result of topology optimization based on CM for Example 2: [0,1000]Hz. **b** The converged result of topology optimization based on MAM for Example 2: [0,1000]Hz

Table 7 Performance results of topology optimization based on MAM and CM for Example 2: [0,50]Hz

Method	Initial objective value	Converged objective value	CPU time(s)	Iteration number
MAM	88952.72	3745.61	3459.68	153
CM	88949.26	3749.18	833.04	148

$$\int_{\tilde{\omega}_{q-1}}^{\tilde{\omega}_q} \|J(\omega)\| d\omega \approx \frac{\tilde{\omega}_q - \tilde{\omega}_{q-1}}{2} \sum_{k=1}^{N} \gamma_k \left\| J\left(\frac{\tilde{\omega}_q - \tilde{\omega}_{q-1}}{2} \mu_k + \frac{\tilde{\omega}_q + \tilde{\omega}_{q-1}}{2} \right) \right\| \tag{27}$$

where $[\tilde{\omega}_{q-1}, \tilde{\omega}_q]$ is one of the previously mentioned subdivisions, γ_k is the weight factor for the kth Gaussian point, and μ_k is the Gaussian point, N is the number of Gaussian points, $N = 16$ is chosen in the paper.

So the integral in a frequency interval can be formulated as follow

$$\int_0^{\omega_f} \|J(\omega)\| d\omega = \sum_{q=1}^{p} \int_{\tilde{\omega}_{q-1}}^{\tilde{\omega}_q} \|J(\omega)\| d\omega \tag{28}$$

where the number p depends on the number of eigenfrequencies in the frequency interval $[0, \omega_f]$.

In this paper, Polynomial Interpolation Scheme (PIS) (Zhu et al. 2010) is chosen to prevent the appearance of localized modes.

$$\begin{aligned}
\mathbf{k}_e &= \frac{15\rho_e^5 + \rho_e}{16} \mathbf{k}_{e0}\\
\mathbf{m}_e &= \rho_e \mathbf{m}_{e0}
\end{aligned} \tag{29}$$

where $\mathbf{k}_e$, $\mathbf{m}_e$ are the element stiffness matrix and mass matrix of element e, respectively, and $\mathbf{k}_{e0}$, $\mathbf{m}_{e0}$ are the stiffness matrix and mass matrix referring to an element density equal to 1.

We assume that harmonic loads are independent of design variables. Liu et al. (2015) applied direct method to analyze sensitivities of an objective function which involves computation of eigenvector derivatives. Such a computation with repeated eigenvalues is a complicated subject (Wu et al. 2015a) and accuracy of eigenvectors derivatives obtained by using the mode superposition

Table 8 Performance results of topology optimization based on MAM and CM for Example 2: [0,500]Hz

Method	Initial objective value	Converged objective value	CPU time(s)	Iteration number
MAM	946688.78	46883.10	6785.59	189
CM	964493.25	46545.33	4868.36	196

Table 9 Performance results of topology optimization based on MAM and CM for Example 2: [0,1000]Hz

Method	Initial objective value	Converged objective value	CPU time(s)	Iteration number
MAM	1515221.09	92560.49	14345.95	243
CM	1567650.59	89348.93	13857.13	290

technique is not ensured. AVM is an alternative to avoid this complication. Yoon (2010) computed the sensitivities by using AVM and model reduction schemes. The sensitivity of objective function in (24) with respect to the material density ρ_e is given by

$$\begin{aligned}\int_0^{\omega_f}\frac{\partial\|J(\omega)\|}{\partial\rho_e}d\omega &= \int_0^{\omega_f}\frac{\partial\sqrt{\overline{J}(\omega)J(\omega)}}{\partial\rho_e}d\omega \\ &= \int_0^{\omega_f}\frac{\overline{J}(\omega)\frac{\partial J(\omega)}{\partial\rho_e}+\frac{\partial\overline{J}(\omega)}{\partial\rho_e}J(\omega)}{2\sqrt{\overline{J}(\omega)J(\omega)}}d\omega\end{aligned} \tag{30}$$

where $\frac{\partial J(\omega)}{\partial\rho_e}$ can be derived as follows

$$\frac{\partial J(\omega)}{\partial\rho_e}=\frac{\partial\left(\mathbf{L}^{\mathrm{T}}\mathbf{x}(\omega)\right)}{\partial\rho_e}=\mathbf{L}^{\mathrm{T}}\frac{\partial\mathbf{x}(\omega)}{\partial\rho_e} \tag{31}$$

The differentiation of (2) with respect to ρ_e gives

$$\frac{\partial\mathbf{S}}{\partial\rho_e}\mathbf{x}(\omega)+\mathbf{S}\frac{\partial\mathbf{x}(\omega)}{\partial\rho_e}=0 \tag{32}$$

where $\mathbf{S}=\mathbf{K}+i\omega\mathbf{C}-\omega^2\mathbf{M}$ is defined as dynamic stiffness matrix (Bathe 2014). Use of (32) yields

$$\frac{\partial\mathbf{x}(\omega)}{\partial\rho_e}=-\mathbf{S}^{-1}\frac{\partial\mathbf{S}}{\partial\rho_e}\mathbf{x}(\omega) \tag{33}$$

Substituting (33) into (31) and noting that $\mathbf{S}$ is a symmetric matrix result in the sensitivity as follows

$$\begin{aligned}\frac{\partial J(\omega)}{\partial\rho_e}&=\mathbf{L}^{\mathrm{T}}\frac{\partial\mathbf{x}(\omega)}{\partial\rho_e}=-\mathbf{L}^{\mathrm{T}}\mathbf{S}^{-1}\frac{\partial\mathbf{S}}{\partial\rho_e}\mathbf{x}(\omega)\\ &=-\boldsymbol{\lambda}^{\mathrm{T}}\frac{\partial\mathbf{S}}{\partial\rho_e}\mathbf{x}(\omega)\end{aligned} \tag{34}$$

where $\boldsymbol{\lambda}$ is the solution of following equation and is called adjoint variable vector

Table 11 Details of time distribution for computing harmonic response by MAM at the initial step for the three frequency intervals in Example 2

Frequency interval	Number of lower modes	Solution of the eigenproblem(s)	Solution of (22)(s)	Total(s)
[0,50]Hz	20	5.805	0.032	5.837
[0,500]Hz	20	5.922	0.225	6.147
[0,1000]Hz	20	5.868	0.632	6.500

$$\mathbf{S}\boldsymbol{\lambda}=\mathbf{L} \tag{35}$$

which can be obtained by using the methods in Section 2 and replacing $\mathbf{F}$ with $\mathbf{L}$. For the problem of dynamic compliance, there is no need to solve the (35) again, since the adjoint variable vector $\boldsymbol{\lambda}$ is the same as the response vector $\mathbf{x}(\omega)$.

The flow chart of the optimization procedure is shown in Fig. 1.

4 Numerical examples

In this section, three examples are given to illustrate the efficiency of the proposed method. The filtering technique (Sigmund 1997) is used to avoid the checkboard pattern. The GCMMA algorithm (Svanberg 2002) is applied as the optimizer. The computations of all examples are completed on a server with Intel CPU Xeon E5-2687 W v4, 128G RAM. The stiffness and mass matrices are stored in the compressed sparse row format. All computations are based on the Intel Math Kernel Library 10.3. The compiler is Intel Visual Fortran Compiler XE 2011. In all examples, we set the error tolerance $\varepsilon=10^{-8}$ of PCG, Young's modulus $E=2\times10^{11}$Pa, Poisson's ratio $\upsilon=0.3$, mass density $\rho=7800\mathrm{kg/m}^3$, proportional damping coefficients $\alpha=10^{-2}$and $\beta=10^{-4}$. The convergence criteria of optimization procedure is set to $\frac{\|g_{k+1}-g_k\|}{\|g_k\|}<10^{-4}$, where g_k is the objective value of kth step. Let $\mathbf{d}_{\mathrm{MAM}}$, $\mathbf{d}_{\mathrm{CM}}$ and $\mathbf{d}_{\mathrm{FM}}$ are the sensitivity vectors at the initial step obtained by AVM based on MAM, CM and FM, respectively. The relative errors of the first two approximations are defined by $\frac{\|\mathbf{d}_{\mathrm{MAM}}-\mathbf{d}_{\mathrm{FM}}\|_2}{\|\mathbf{d}_{\mathrm{FM}}\|_2}$ and $\frac{\|\mathbf{d}_{\mathrm{CM}}-\mathbf{d}_{\mathrm{FM}}\|_2}{\|\mathbf{d}_{\mathrm{FM}}\|_2}$. Let $\boldsymbol{\rho}_{\mathrm{MAM}}$ and $\boldsymbol{\rho}_{\mathrm{CM}}$ represent the converged design variable vectors obtained by

Table 10 Details of time distribution for computing harmonic response by CM at the initial step for the three frequency intervals in Example 2

Frequency interval	Sturm sequence(s)	Number of lower modes	Solution of the eigenproblem(s)	PCG method(s)	Calculation of (14) and (16)(s)	Total(s)
[0,50]Hz	0.545	1	0.710	0.065	0.091	1.411
[0,500]Hz	0.532	5	2.006	0.084	0.519	3.141
[0,1000]Hz	0.620	10	3.207	0.166	1.386	5.379

Table 12 The relative errors of the sensitivity analyses based on CM and MAM at the initial step

Method	[0,50]Hz	[0,500]Hz	[0,1000]Hz
CM	6.625e-09	9.844e-09	3.574e-09
MAM	6.791e-04	7.810e-02	0.4534

using MAM and CM, respectively. The relative difference between $\boldsymbol{\rho}_{MAM}$ and $\boldsymbol{\rho}_{CM}$ is defined as $\frac{\|\boldsymbol{\rho}_{MAM}-\boldsymbol{\rho}_{CM}\|_2}{\|\boldsymbol{\rho}_{CM}\|_2}$. The first $n_d = 20$ modes are employed in MAM. The subspace iteration method is used to solve the eigenproblem.

Example 1 Minimization of the displacement amplitude at a certain DOF for a 2D cantilever beam structure.

The design domain of the beam structure is a rectangle of size 2m × 1m with 0.01m thickness and it is clamped at the left side as shown in Fig. 2. The structure is meshed into 200 × 100 2D 4-node plane stress elements and has 40,400 DOFs. The volume fraction is constrained to be less than 30%. A harmonic load with amplitude 10kN is applied at the center of the right edge. Three frequency intervals [0,50]Hz, [0,100]Hz, and [0,500]Hz are considered. The objective function is the integral of vertical displacement amplitude at the loading position over given frequency intervals. The filter radius is set to 4.

For the three frequency intervals, 128, 144, and 608 Gaussian frequency points are determined, respectively, at the initial step. The converged results of topology optimization based on CM and MAM for [0,50]Hz, [0,100]Hz, and [0,500]Hz are shown in Figs. 3(a,b), 4(a,b), and 5(a,b), respectively. It is seen that there are no siginificant difference of the optimized configurations of the structure based on the two methods. Details of optimization are listed in Tables 1, 2 and 3. From these tables, it can be found that the topology optimizations based on CM can reduce 70.19%, 65.51% and 21.90%

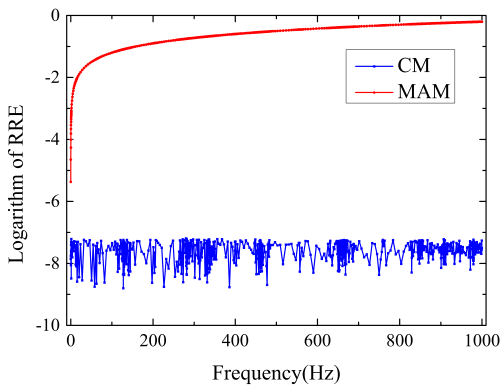

Fig. 12 The comparison of RREs of harmonic responses using MAM and CM at the initial step for Example 2: [0,1000]Hz

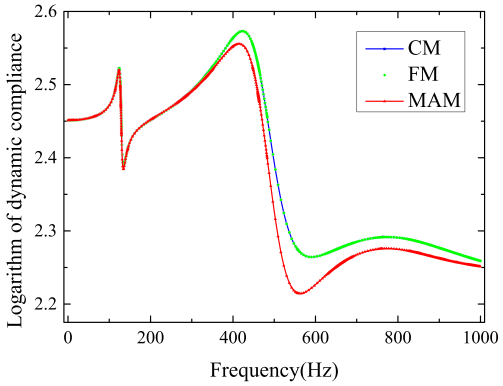

Fig. 13 The comparison of dynamic compliances based on MAM and CM at the initial step for Example 2: [0,1000]Hz

CPU time, respectively, compared with those based on MAM. Details of time distribution for computing harmonic response by CM and MAM at the initial step for the three frequency intervals are list in Tables 4 and 5, respectively. The comparison of RREs of harmonic response analysis based on the two methods for [0,500]Hz at the initial step is given in Fig.6. The figure shows that attempts to increase n_d from 20 to 50 are unlikely to cause a remarkable improvement of RRE. But $n_d = 50$ will cost much more CPU time than $n_d = 20$ in MAM. It can also demonstrate that the RRE of CM is less than $10^{-7.3}$ at all Gaussian frequency points. The RRE of MAM sharply increases from $10^{-5.8}$ to $10^{-0.5}$ as the excitation frequency increases. At the initial step, the sensitivity analyses computed by CM and MAM, respectively, are compared with that by FM. The relative errors are list in Table 6. It can be observed that MAM cannot ensure the accuracy for a large range of excitation frequency. Fig. 7 displays variation of vertical displacement amplitude at the loading position, i.e. the user-defined DOF, in frequency interval [0,500]Hz at the initial setp. Additionally, the result of the FM is also plotted in Fig. 7 for comparison. It can be observed that increasing number of modes in MAM will have little influence of the displacement amplitude. The

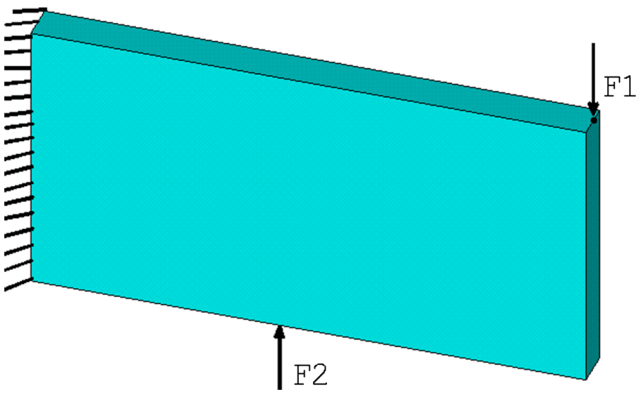

Fig. 14 3D left clamped structure

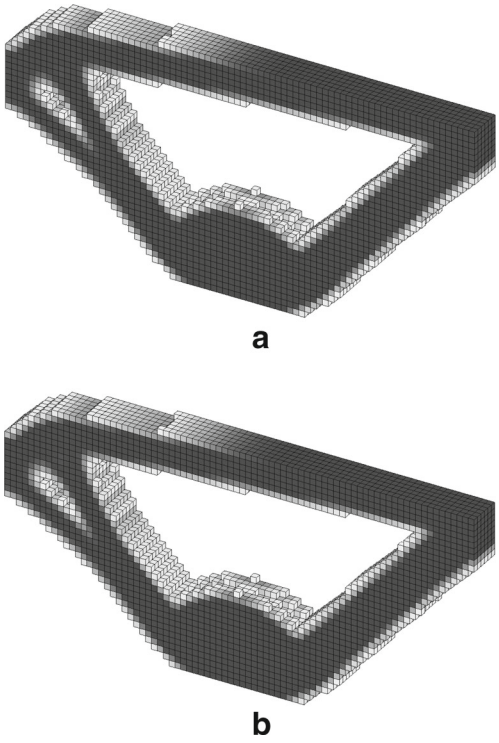

Fig. 15 **a** The converged result of topology optimization based on CM for Example 3: [0,50]Hz. **b** The converged result of topology optimization based on MAM for Example 3: [0,50]Hz

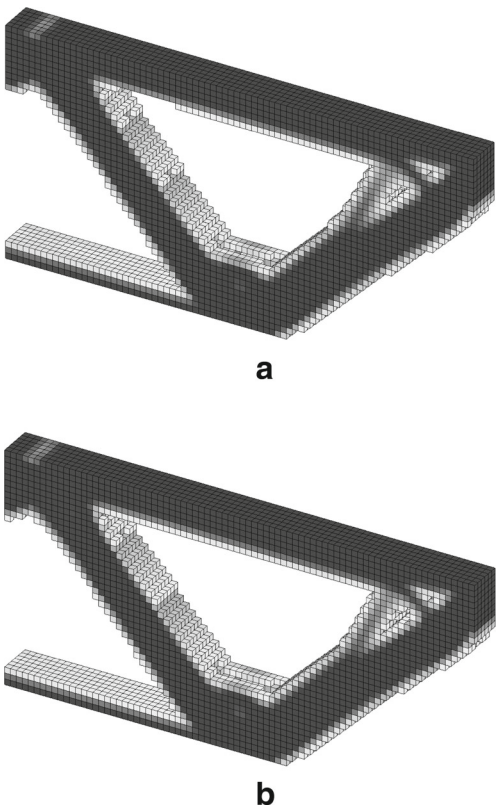

Fig. 16 **a** The converged result of topology optimization based on CM for Example 3: [0,300]Hz. **b** The converged result of topology optimization based on MAM for Example 3: [0,300]Hz

Table 13 Performance results of topology optimization based on MAM and CM for Example 3: [0,50]Hz

Method	Initial objective value	Converged objective value	CPU time(s)	Iteration number
MAM	1636.85	76.43	13,641.88	79
CM	1636.68	76.42	6500.61	79

relative difference between the converged design variable vectors based on MAM and CM for the three frequency intervals are 0.06, 0.09 and 0.08, respectively.

Example 2 Minimization of the dynamic compliance of a 2D beam structure.

The structure has design domain of a rectangle of size $2\text{m} \times 0.5\text{m}$ with 0.01m thickness and is clamped-clamped as shown in Fig. 8. It is meshed into 200×50 2D 4-Node plane stress elements with 20,298 DOFs. The volume fraction is constrained to be less than 30%. Three harmonic forces are applied at quarter, center and three quarters points of the bottom edge with amplitudes $F1 = F2 = F3 = 10\text{kN}$, F1 and F3 have phase difference of 180 degrees from F2. Three frequency intervals [0,50]Hz, [0,500]Hz and [0,1000]Hz are considered. The objective function is integral of the dynamic compliance under given frequency intervals. The filter radius is set to 2.

For the three frequency intervals, 48, 432 and 912 Gaussian frequency points are calculated at the initial step respectively. The converged results of topology optimization based on CM and MAM for [0,50]Hz, [0,500]Hz and [0,1000]Hz are shown in Figs. 9(a,b), 10(a,b) and 11(a,b), respectively. From Figs.10(a,b) and 11(a,b), it is found that the converged results of the topology optimization based on MAM and CM have some differences, which result from lacking of accuracy of MAM at higher excitation frequencies ω. Performance results of topology optimization based on MAM and CM are shown in Tables 7, 8 and 9. From Tables 7, 8, 9, it can be observed that the optimization via CM can reduce 75.92%, 28.25% and 3.41% CPU time, respectively, compared with those via MAM.

Table 14 Performance results of topology optimization based on MAM and CM for Example 3: [0,300]Hz

Method	Initial objective value	Converged objective value	CPU time(s)	Iteration number
MAM	9841.82	452.05	26833.95	83
CM	9816.94	452.09	17162.51	76

Table 15 Details of time distribution for computing harmonic response by CM at the initial step for the two frequency intervals in Example 3

Frequency interval	Sturm sequence(s)	Number of lower modes	Solution of the eigenproblem(s)	PCG method(s)	Calculation of (14) and (16)(s)	Total(s)
[0,50]Hz	3.669	2	5.492	0.661	0.835	10.657
[0,300]Hz	3.801	6	9.665	1.982	4.138	19.586

Details of time distribution for computing harmonic response by CM and MAM at the initial step for the three frequency intervals are list in Tables 10 and 11, respectively. For the case of frequency interval [0,1000]Hz, the topology optimizations via the two methods converge to different configurations. Although CM only costs 3.41% CPU time less than MAM, CM costs much less average CPU time than MAM for per iteration, as shown in Table 9. At the first step, the sensitivity analysed by CM and MAM are compared with that by FM, see Table 12. The errors in sensitivity analysis can cause the optimization to converge to different configurations. The relative difference between the converged design variable vectors by MAM and CM for the three frequency intervals is 0.02, 0.25 and 0.5, respectively. The comparison of RREs of harmonic responses based on the two methods for [0,1000]Hz at the initial step is given in the Fig.12. The figure demonstrates that the RRE of CM is less than $10^{-7.1}$ at all Gaussian frequency points. The RRE of MAM sharply increases from $10^{-5.4}$ to $10^{-0.2}$ as the excitation frequency increases. The comparison of dynamic compliance based on MAM, CM and FM at initial step for [0,1000]Hz is plotted in Fig.13. Obviously, the difference is more significant at higher excitation frequency ω.

Example 3 Minimization of the dynamic compliance of a 3D structure.

The structure has the design domain of size $0.8\text{m} \times 0.4\text{m} \times 0.06\text{m}$ and is clamped at the left side as shown in Fig. 14. It is meshed into $80 \times 40 \times 6$ 3D 8-Node solid elements with 68,880 DOFs. Two harmonic forces are applied at center of the bottom surface, and center of the intersection line of the upper surface and the right surface, respectively, with amplitude $F1 = 0.5 \times F2 = 5\text{kN}$. In addition, F1 has a phase difference of 180 degrees from F2. Two frequency intervals [0,50]Hz, and [0,300]Hz are considered. The volume fraction is constrained to be less than 40%. The objective function is integral of dynamic compliance under the given frequency intervals. The filter radius is set to 2.

For the two frequency intervals, 144 and 512 Gaussian frequency points are calculated at the initial step, respectively. The converged results of topology optimization based on CM and MAM for [0,50]Hz and [0,300]Hz are plotted in Figs.15(a,b) and 16(a,b), respectively. Performance results of topology optimization based on MAM and CM are listed in Tables 13 and 14. It can be seen that the optimizations based on CM can reduce 52.35% and 36.04% CPU time, respectively, compared with MAM. Details of time distribution for computing harmonic response by CM and MAM at the initial step for the two frequency intervals are list in Tables 15 and 16, respectively. At the first step, the sensitivity analyses by CM and MAM are compared with that by FM, see Table 17. The comparison of RREs of harmonic responses using MAM and CM for [0,300]Hz at the initial step is plotted in the Fig.17. The figure indicates that the RRE of CM is less than $10^{-7.3}$ at all Gaussian frequency points. The RRE of MAM sharply increases from $10^{-6.1}$ to $10^{-0.7}$ as the excitation frequency increases. The comparison of dynamic compliance based MAM, CM and FM for [0,300]Hz at the initial step is displayed in Fig. 18, which illustrates that, for MAM, harmonic response under higher excitation ω is less accurate. The relative difference between the converged design variable vectors based on MAM and CM for the two frequency intervals is 0.002 and 0.04, respectively.

Based on the three examples above, it can be concluded that, in terms of efficiency and accuracy, the topology optimization method based on the CM is the

Table 16 Details of time distribution for computing harmonic response by MAM at the initial step for the two frequency intervals in Example 3

Frequency interval	Number of lower modes	Solution of the eigenproblem(s)	Solution of (22)(s)	Total(s)
[0,50]Hz	20	37.107	0.433	37.540
[0,300]Hz	20	37.804	1.300	38.100

Table 17 The relative errors of the sensitivity analyses based on CM and MAM at the initial step for Example 3

Method	[0,50]Hz	[0,300]Hz
CM	6.060e-9	7.614e-9
MAM	7.699e-4	2.901e-2

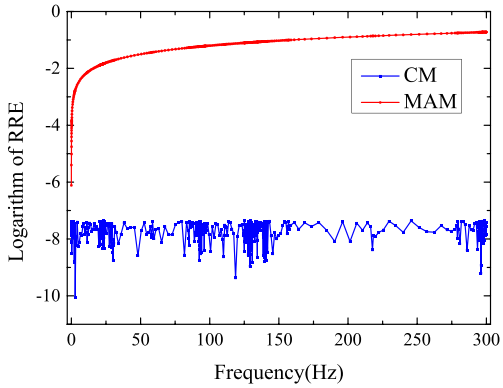

Fig. 17 The comparison of RREs of harmonic responses using MAM and CM at the initial step for Example 3: [0,300]Hz

best one among these methods. This is mainly because of the integral function and its derivatives as shown in (25), (34) and (35), respectively, can be fast and exactly computed by using CM of harmonic response analysis.

5 Conclusions

In this paper, the CM method for harmonic response analysis has been integrated to structural topology optimization related to harmonic responses. The CM is based on modal superposition and model order reduction. Contrasted with MAM, usually adopted in the topology optimization, the CM determines the number of lower eigenfrequencies and eigenvectors for modal superposition quantitatively and improves the accuracy by using MOR. Due to the accuracy of the CM, the sensitivity analysis results of objective functions are more reliable. Three examples are investigated by using topology optimization based on MAM and CM, respectively. For both problems of minimizing the dynamic compliance and minimizing the displacement amplitude at a given DOF, the topology optimization based on the CM not only guarantee the accuracy of results, but also reduce CPU time remarkably.

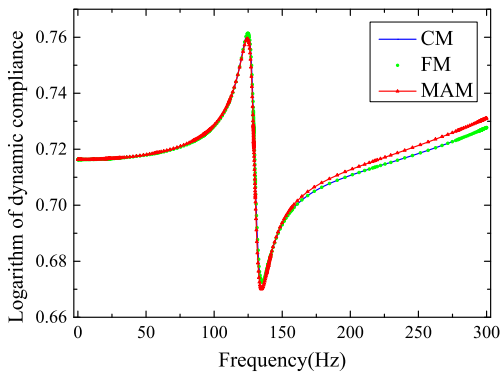

Fig. 18 The comparison of dynamic compliances based on MAM and CM at the initial step for Example 3: [0,300]Hz

Acknowledgments The authors are grateful to Krister Svanberg for providing the Matlab code of GCMMA optimizer. The work was supported by the National Natural Science Foundation of China (Grant No. 11672118).

References

Bathe K-J (2013) The subspace iteration method – revisited. Comput Struct 126:177–183

Bathe K-J (2014) Finite Element Procedures, second ed. Prentice Hall, Watertown

Bendsøe MP, Kikuchi N (1988) Generating optimal topologies in structural design using a homogenization method. Comput Methods Appl Mech Eng 71:197–224

Bendsøe MP, Sigmund O (2004). Topology Optimization: theory, methods, and applications, second ed. Springer, Berlin

Deaton JD, Grandhi RV (2014) A survey of structural and multidisciplinary continuum topology optimization: post 2000. Struct Multidiscip Optim 49:1–38

Díaz AR, Kikuchi N (1992) Solutions to shape and topology eigenvalue optimization problems using a homogenization method. Int J Numer Methods Eng 35:1487–1502

Dickens JM, Nakagawa JM, Wittbrodt MJ (1997) A critique of mode acceleration and modal truncation augmentation methods for modal response analysis. Comput Struct 62:985–998

Du J, Olhoff N (2007) Topological design of freely vibrating continuum structures for maximum values of simple and multiple eigenfrequencies and frequency gaps. Struct Multidiscip Optim 34:91–110

Golub GH, Van Loan CF (2013). Matrix Computations, forth ed. Johns Hopkins University Press, Baltimore

Grimes RG, Lewis JG, Simon HD (1994) A shifted block Lanczos algorithm for solving sparse symmetric generalized eigenproblems. SIAM J Matrix Anal Appl 15:228–272

Haftka RT, Gürdal Z (1992). Elements of Structural Optimization, third ed. Kluwer, Dordrecht

Jensen JS (2007) Topology optimization of dynamics problems with Padé approximants. Int J Numer Methods Eng 72:1605–1630

Jog CS (2002) Topology design of structures subjected to periodic loading. J Sound Vib 253:687–709

Kang Z, Zhang XP, Jiang SG, Cheng GD (2012) On topology optimization of damping layer in shell structures under harmonic excitations. Struct Multidiscip Optim 46:51–67

Liu H, Zhang WH, Gao T (2015) A comparative study of dynamic analysis methods for structural topology optimization under harmonic force excitations. Struct Multidiscip Optim 51:1321–1333

Ma ZD, Kikuchi N, Cheng HC (1995) Topological design for vibrating structures. Comput Methods Appl Mech Eng 121:259–280

Olhoff N, Du J (2005) Topological design of continuum structures subjected to forced vibration. Proceedings of 6th world congresses of structural and multidisciplinary optimization, Rio de Janeiro, Brazil

Pedersen NL (2000) Maximization of eigenvalues using topology optimization. Struct Multidiscip Optim 20:2–11

Shu L, Wang MY, Fang ZD, Ma ZD, Wei P (2011) Level set based structural topology optimization for minimizing frequency response. J Sound Vib 330:5820–5834

Sigmund O (1997) On the Design of Compliant Mechanisms Using Topology Optimization. Mech Struct Mach 25:493–524

Svanberg K (2002) A class of globally convergent optimization methods based on conservative convex separable approximations. SIAM J Optim 12:555–573

Tcherniak D (2002) Topology optimization of resonating structures using SIMP method. Int J Numer Methods Eng 54:1605–1622

Wu BS, Yang ST, Li ZG, Zheng SP (2015a) A preconditioned conjugate gradient method for computing eigenvector derivatives with distinct and repeated eigenvalues. Mech Syst Signal Process 50:249–259

Wu BS, Yang ST, Li ZG, Zheng SP (2015b) A combined method for computing frequency responses of proportionally damped systems. Mech Syst Signal Process 60-61:535–546

Wu BS, Yang ST, Li ZG (2016) An algorithm for solving frequency responses of a system with Rayleigh damping. Arch Appl Mech 86:1231–1245

Yoon GH (2010) Structural topology optimization for frequency response problem using model reduction schemes. Comput Methods Appl Mech Eng 199:1744–1763

Yu Y, Jang IG, Kwak BM (2013) Topology optimization for a frequency response and its application to a violin bridge. Struct Multidiscip Optim 48:627–636

Zhao JP, Wang CJ (2016) Dynamic response topology optimization in the time domain using model reduction method. Struct Multidiscip Optim 53:101–114

Zhu JH, Beckers P, Zhang WH (2010) On the multi-component layout design with inertial force. J Comput Appl Math 234:2222–2230

Zhu JH, He F, Liu T, Zhang WH (2017) Structural topology optimization under harmonic base acceleration excitations. Struct Multidiscip Optim. https://doi.org/10.1007/s00158-017-1795-0